Chapter 5

EUV/Soft X-Ray Interference Lithography

Shumin Yang and Yanqing Wu

Additional information is available at the end of the chapter

http://dx.doi.org/10.5772/intechopen.74564

Abstract

Based on the coherent radiation from an undulator source, extreme UV interference lithography (EUV-IL) technology is considered as the leading candidate for future nodes of high-volume semiconductor manufacturing. The throughput of this technique is much higher than that of traditional lithography methods such as e-beam lithography (EBL) and laser interference lithography (LIL). Different types of interference schemes based on reflection mirrors and transmission diffraction masks have been described in this chapter. Achromatic Talbot lithography (ATL) and the soft X-ray interference lithography (SXIL) with different photon energies have also been developed to produce highly dense, high-resolution periodic nanostructures. Two scan-exposure techniques, one is the method employing the broadband Talbot effect and the other based on the multi-grating EUV-IL with an order sorting aperture (OSA), have been used to obtain periodic nanostructures over large areas. Applications of EUV-IL on EUV-resist testing and nano-science have been illustrated.

Keywords: EUV, interference lithography, achromatic Talbot lithography, soft X-ray interference lithography, periodic nanostructures

1. Introduction

1.1. EUV interference lithography

Based on the coherent radiation from an undulator source, extreme ultraviolet interference lithography (EUV-IL) has been proven to be a powerful tool for high-resolution periodic nanostructure fabrication. The throughput of this technique is much higher than that of traditional lithography methods such as e-beam lithography (EBL) and laser interference lithography (LIL). Based on the interference of two or more coherent beams, interference lithography (IL) is usually used as a simple

method for large-area periodic nanostructure fabrication. Through a combination of advantages of IL and the short wavelength of EUV, EUV-IL technology has been proved as a powerful tool for high-resolution nanostructure fabrication over large areas. So far, several EUV-IL beamlines have been built in different synchrotron facilities, such as the XILII beamline in swiss light source (SLS) [1], the EUV-IL beamline in shanghai synchrotron radiation facility (SSRF) [2], the EUV-IL beamline in New SUBARU synchrotron radiation facility [3], the EUV-IL beamline at the University of Wisconsin-Madison [4] and the EUV-IL beamline in the national synchrotron radiation research center (NSRRC), Taiwan [5]. Up to now, the highest-resolution line structures with 6-nm half pitch (HP) have been afforded in PSI XILII [1]. During the last decade, a number of interference schemes were investigated including Lloyd's mirror, two-grating and multi-grating schemes.

1.2. Different types of EUV-IL

1.2.1. Interference with reflection optics

Figure 1a illustrates the general scheme of a Lloyd's mirror interferometer. The single-plane mirror is the key component in the interference scheme. A part of the incident beam is reflected by this mirror which interferes with the unreflected part of the beam to form interference fringes. Line structures with periods as small as 38 nm have been fabricated by this method at the Synchrotron Radiation Center (SRC), as shown in **Figure 1b** [6, 7]. Mirrors coated by the resonance multilayer are often used to split and reflect the soft X-rays. The extremely high requirements on mirror surface quality and the limited coherence of the soft X-ray sources complicate the implementation of such interferometers.

1.2.2. Interference with diffraction optics

Figure 2 illustrates the general scheme of the IL method with transmission diffraction optics. Under normal illumination from a spatially coherent EUV source, diffracted beams through the transmission mask interfere together at a certain distance from the mask. Line-space structures and 2D periodic structures will be fabricated by the two- and four-beam transmission

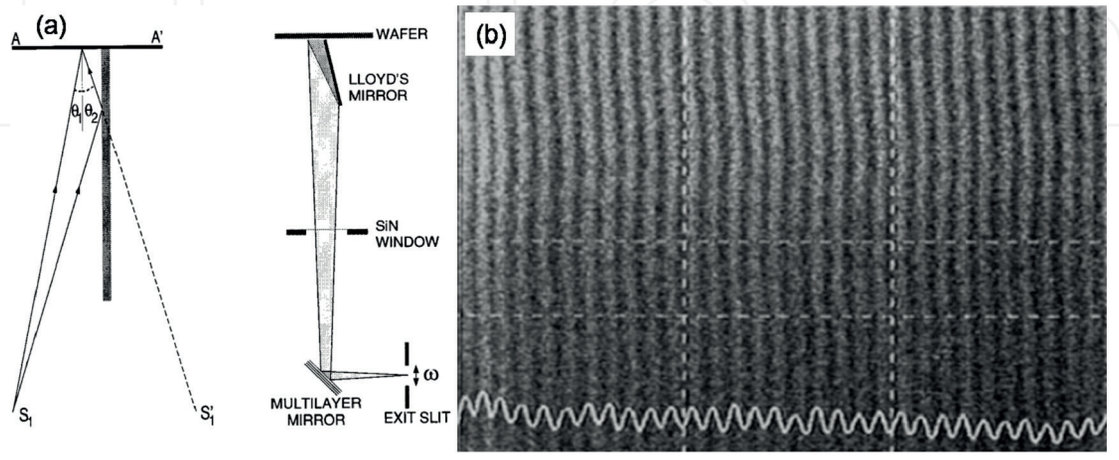

Figure 1. (a) The general scheme of a Lloyd's mirror interferometer. (b) Line structures with 38-nm period fabricated by SRC using the Lloyd's mirror interferometer (reproduced from [6], with the permission of AIP publishing).

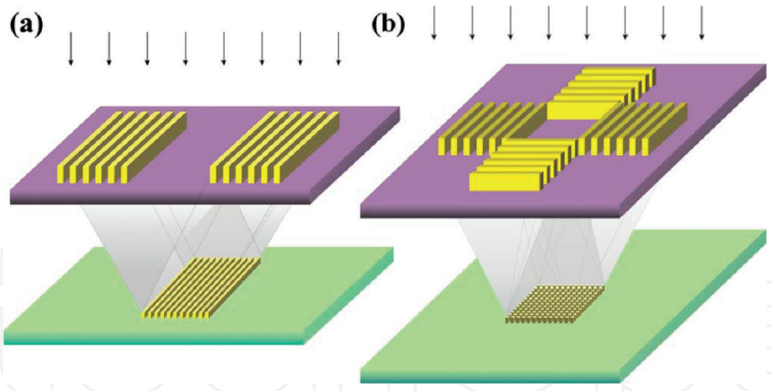

Figure 2. The general scheme of the two-beam (a) and four-beam (b) transmission-diffraction IL method (reproduced with permission from [8] ©(2009) COPYRIGHT Society of Photo-Optical Instrumentation Engineers (SPIE)).

diffraction IL method [8]. The period of the fringe pattern is related to the mother gratings that generate the fringe pattern [9, 10]. For the two-beam diffraction method, the incident beam is diffracted by each grating in certain angles, θm, given by: $\sin\theta m = m\lambda/Pg$, where m is the diffraction order and Pg is grating periodicity. When the two gratings are illuminated with the same beam intensity, in the area where the diffracted beams interfere, the periodicity, P, of the aerial image is given by: P=Pg/2 m. Due to the lower diffraction efficiency of diffraction with higher order, only the 1rd diffraction is used for the usual two-beam interference lithography. Thus, the periodicity of the interference beams is given by: P=Pg/2. For the four-beam diffraction method, the periodicity of the interference beams is given by: $P=Pg/\sqrt{2}$.

Grating is one of the key parts of the XIL techniques. Dry-etching and lift-off processes are usually used for the grating fabrication process. Smooth and steep Cr or Au line structure can be fabricated by using the dry-etching process. However, a poisonous gas such as Cl_2 is usually used during the dry-etching process. Cr grating with 80-nm line period has been fabricated by this process. And line structures with 40-nm period have been printed in a calixarene

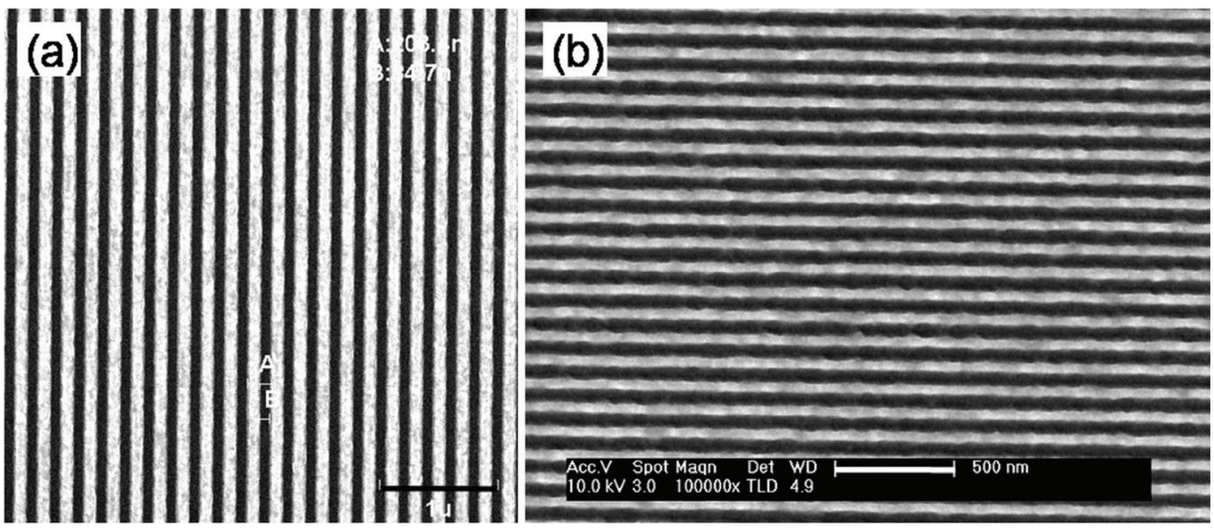

Figure 3. (a) An SEM image of the two beam grating and (b) an SEM image of the exposure result on PMMA resist. The scale bars are 1000 nm in (a) and 500 nm in (b).

negative resist at the XIL II beamline in PSI [11]. By means of electron beam evaporation and lift-off processes, smooth Au line structure can also be fabricated. An Au grating with 200-nm line period has been fabricated by this process, **Figure 3a**. And line structures with 100-nm period have been printed in PMMA resist at the XIL beamline in SSRF, **Figure 3b**.

2. Broad bandwidth IL based on synchrotron radiation source

2.1. BW multi-grating EUV-IL

2D nanopatterns such as s holes, posts, sparse hole arrays or rings can be obtained when the number of interference beams exceeds three. The resultant pattern intensity depends strongly on the relative phases of the beams. Versatile periodic nanostructures can be obtained by changing the number of interfering beams and by controlling the relative phases of the beams [10]. **Figure 4** illustrates the principle of the four-beam interference lithography. The transmission gratings were written on a single mask. The diffracted beams from different gratings overlap to yield a desired pattern. The phases of the diffraction beams are controlled by the precise control of the positions of the gratings, that is, αi, i = 1,⋯, 4, in the figure [10]. Thus, an EBL machine with an interferometer-controlled stage is necessary for the mask-writing process. Two distinct patterns with different contrasts can be obtained in the four-beam case by controlling the phases of the gratings. The incoherent addition of the diffraction beams occurs when $\delta x - \delta y = (n + 1/2)\pi$, where n is an integer and $\delta x = (\alpha 1 - \alpha 2)/2$ and $\delta y = (\alpha 3 - \alpha 4)/2$. The other pattern distribution with high contrast is obtained when $\delta x - \delta y = n\pi$. **Figure 5** illustrates the simulation results demonstrating the influence of phase difference mentioned above during four-beam interference. A four-beam grating with 100 nm is simulated to show

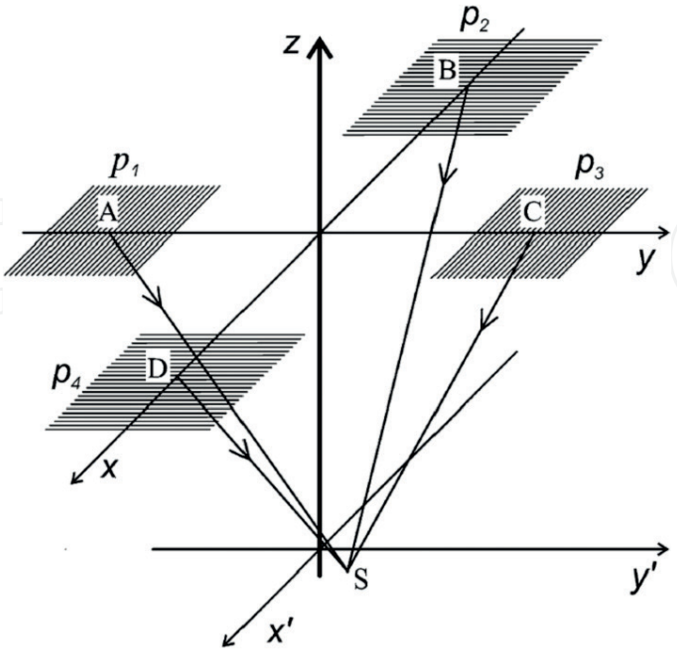

Figure 4. Multiple beam interference lithography with four-beam diffraction gratings (reproduced with permission from [10] ©2005 Elsevier B.V.).

http://dx.doi.org/10.5772/intechopen.74564

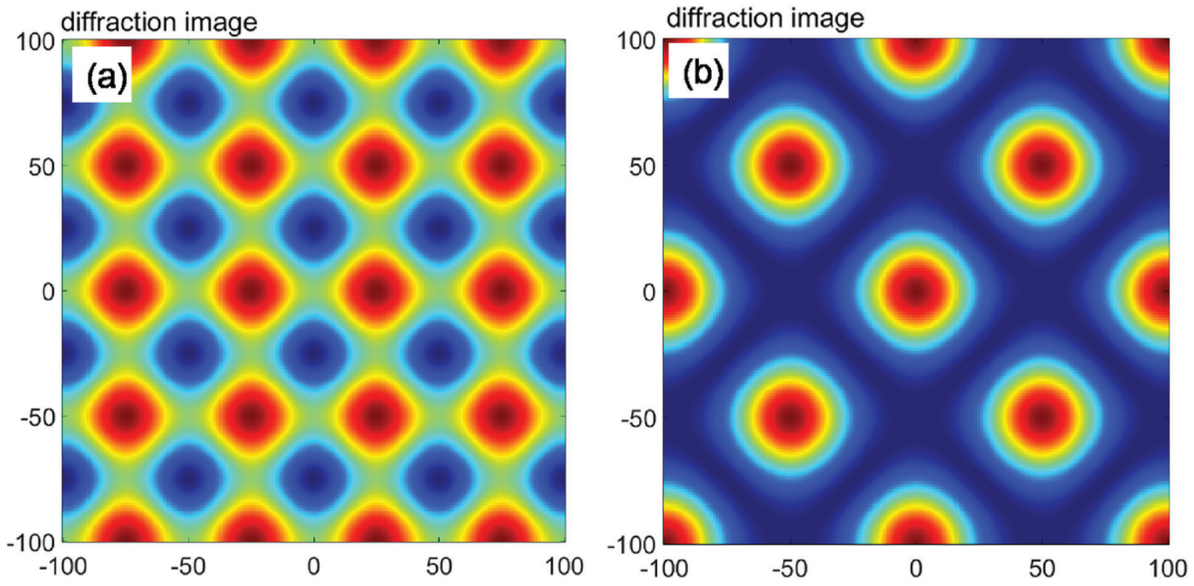

Figure 5. Simulation results demonstrating the influences of phases in four-beam interference. (a) $\delta x - \delta y = (n + 1/2)\pi$, the fringe period in the simulation result is 50 nm. (b) $\delta x - \delta y = n\pi$, the fringe period in the simulation result is 70 nm.

the influence of the phase. Square grids with low-intensity contrast in a 50-nm period (p/2) and a high-intensity contrast in a 70-nm period (p/√2) are demonstrated in **Figure 5a** and **5b**.

The exposure results of several masks with different grating arrangements are shown in **Figure 6**. A negative-tone resist, HSQ, was used during exposure. Line-space patterns with 22-nm HP have been obtained by using a typical two-beam grating mask (**Figure 6a**). The exposure of three- and four-beam grating masks will result in hexagonal lattice and square lattice dot arrays in HSQ resist, **Figure 6b** and **6c**. The exposure result of an incoherent illumination mask is shown in **Figure 6d**. Hole arrays with 25-nm HP is obtained in HSQ resist. In this configuration, the two-crossed pair gratings have different periodicities, which resulted in the incoherent addition of the diffraction beams. **Figure 6e** shows a six-grating mask configuration that results in the so-called Kagome lattices [12].

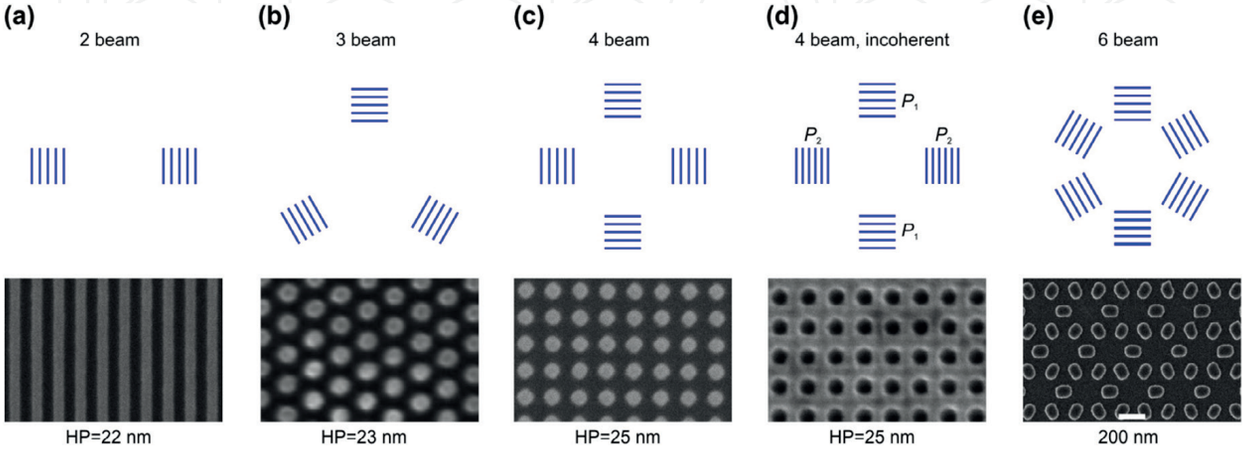

Figure 6. Schematic of different configurations for multiple-beam EUV-IL (first row) and SEM images of corresponding exposures in HSQ photoresist (reproduced with permission from [12] ©2015 Elsevier B.V.).

2.2. Achromatic Talbot lithography

Under monochromatic coherent light illumination, Talbot first noticed that self-images of the gratings were produced at periodic distances away from a transmission diffraction grating [13]. The periodic distance between the self-image planes (Talbot distance, Z_T) is equal to: $Z_T = 2p^2/\lambda$, where p is the grating period and λ is the illumination wavelength. Under the broadband illumination with a spectral bandwidth, the imaging result is very different. Achromatic and stationary patterns of a 1D periodic line structure can be obtained behind the distance $Z_A = 2P^2/\Delta\lambda$ [14]. **Figure 7** shows the scheme of the achromatic and stationary imaging for periodic grating under the broadband illumination with a spectral bandwidth ($\Delta\lambda$). It is called as achromatic spatial frequency multiplication (ASFM) or achromatic Talbot lithography (ATL). The achromatic Talbot distance of the square lattice grid should be $Z_A = 2P^2/\Delta\lambda$, while the achromatic Talbot distance of the hexagonal lattice grid should be $Z_A = 3/2P^2/\Delta\lambda$ [15]. ATL has been proved to be a very robust, highly efficient and simple technique to produce highly dense, high-resolution periodic nanostructures down to 15-nm feature size [16, 17].

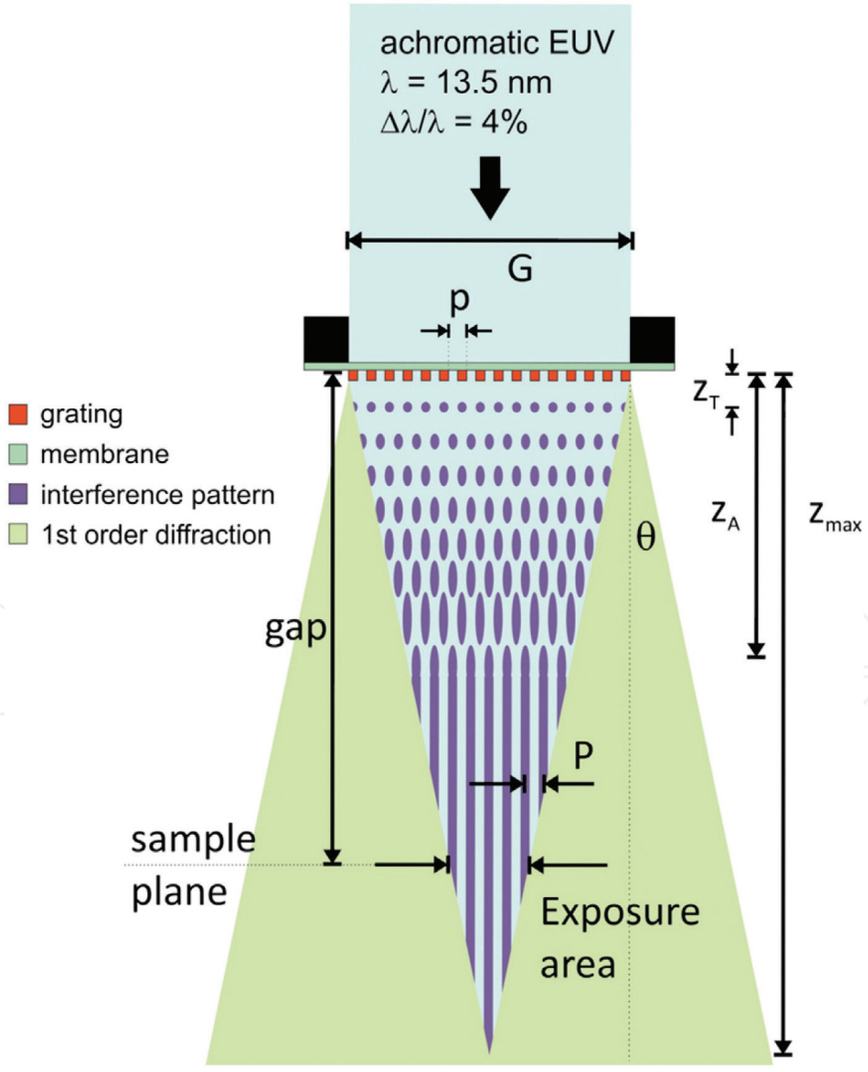

Figure 7. Schematic of the achromatic Talbot lithography. (Reproduced with permission from [16] ©2016 Elsevier B.V.).

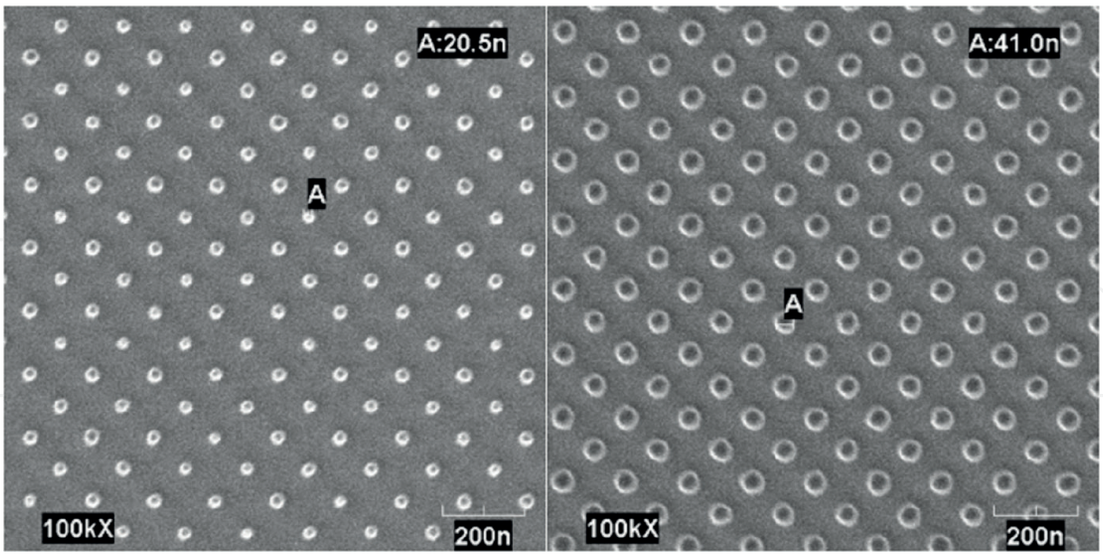

Figure 8. SEM images of the nanodot arrays with dot size at 20 and 40 nm on HSQ resist with a 106-nm period.

During ATL, all of the diffraction orders from different wavelengths overlap together, which makes full use of the beam power. This method is suitable for broadband EUV sources, that is, the majority of EUV sources, and for low-intensity or brightness sources. Two-dimensional periodic patterns in transmission masks with high resolution and uniformity are required to produce dot/hole arrays with high resolution and uniformity. The rectangular transmission grating is very important for the exposure results with high contrast. The nickel or gold electroplating process is utilized to obtain rectangular transmission grating. By using the rectangular transmission grating produced by the nickel electroplating process, nanodot arrays with dot size at 20 and 40 nm in the 106-nm period have been obtained on HSQ resist, as shown in **Figure 8**.

The interference patterns in ATL exposure are much sharper than that in multi-grating IL because there are much more waves with different wave vectors. ATL technique has a long focal length, as well as that of multi-grating one, because of broadband EUV/soft X-rays. However, ATL mask is more difficult to be fabricated than the other since the 0th order light must be blocked completely by the mask.

3. Large-area stitching EUV-IL

Large-area periodic nanostructures are required in many scientific research areas such as nano-magnetics, nano-optics, nano-device fabrication, industrial applications and so on. As mentioned above, large-area periodic nanostructures can be obtained by a single XIL exposure, but the patterned area is limited by the mask area. The area with nanostructures is equal to or less than the area of one grating in the mask. Usually, the grating area is about ~100 × 100 μm^2. This is not large enough for some researches because the spot size of some detecting instruments is already several millimeters. Furthermore, this area is also too small

to fabricate a practical device. Unfortunately, it is difficult to stitch the exposure area one by one because the patterned area is surrounded by the area exposed by the 0th order diffraction beams from the mask.

In order to obtain larger exposure-area nanostructures, two scan-exposure techniques have been developed, one is the method employing the achromatic Talbot lithography [17] and the other is based on the BW multi-grating EUV-IL with an order sorting aperture (OSA) [18, 19].

3.1. Step-and-repeat ATL

Compared with EUV-IL, the exposure area of ATL is very similar to that of the mask area, with only small no-interfering areas left on the four sides of the pattern area [17]. To obtain periodic nanopatterns over a large area, step-and-repeat strategy is utilized during ATL. With step-and-repeat ATL, uniform nanopatterns with high uniformity can be produced in the dimension of fabrication capabilities [17]. As mentioned above, ATL makes full use of the beam power. A few seconds is required during the single-shot ATL exposure over an area of about 500 × 500 μm^2. Using step-and-repeat exposure, 15-nm dot arrays over an area of 1 × 1 cm^2 were obtained in just about 5 min by stitching multiple fields [17]. Line arrays up to 5 × 5 mm^2 have also been fabricated by the beam scanning techniques [20]. Comparing to the beam scanning techniques, ATL with step-and-repeat exposure has its advantages. Mask fabrication above the main writing field size of EBL often has challenges and this exacerbates for 2D patterns such as hole or dot arrays. While during ATL with step-and-repeat method, the full use of the beam power make sure the short exposure time for a single-shot exposure over large area. And the large sinle-shot exposure area with small no interfering areas on the four sides enable the easily step-and repeat stitching of multiple exposure fields. This method enables the fabrications of nanopatterns with high resolution and high throughput over large areas.

3.2. Stitching multi-grating EUV-IL

In an EUV-IL, the 0th order diffraction beams from the mask make stitching of the single-shot exposure area impossible. An OSA and an in-situ alignment system are applied to solve this problem in the XIL beamline at SSRF [18]. To block the 0th order diffraction beams through the mask, the OSA size is larger than the pattern area but less than the distance between the grating pairs, as shown in **Figure 9**. The in-situ alignment system contains two parts: a one-dimensional motion motor which is used along the Z direction to adjust the distance between the OSA and the wafer and a two-dimensional motion stage in the XY direction used to align the position of OSA with respect to the mask. By applying this OSA in-situ alignment system, the 0th order diffraction beams could be blocked effectively and the exposure area could be stitched one by one.

Figure 10 shows the stitching result of a four-beam transmission mask with 170-nm period. The 2D nanostructures are exposed over an exposure area of 2 cm x 2 cm by this stitching method, **Figure 10a**. Stitching gaps with no patterns are also shown in **Figure 10b** with less area. It has

http://dx.doi.org/10.5772/intechopen.74564

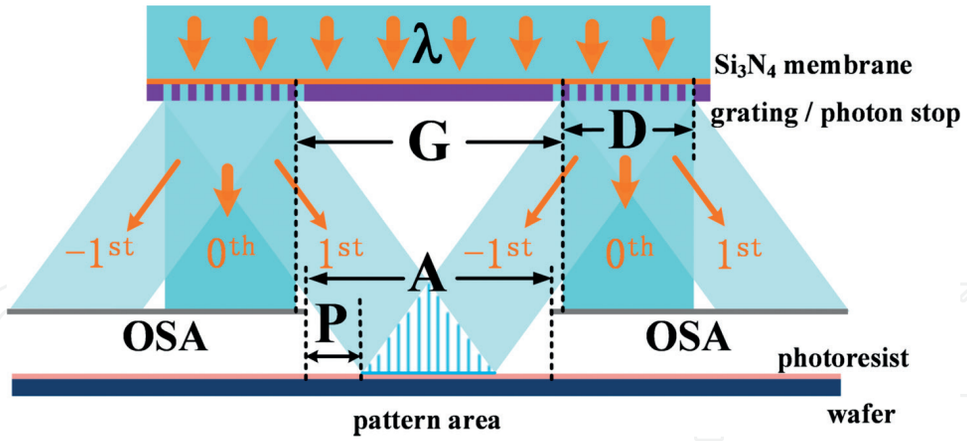

Figure 9. OSA schematic diagram.

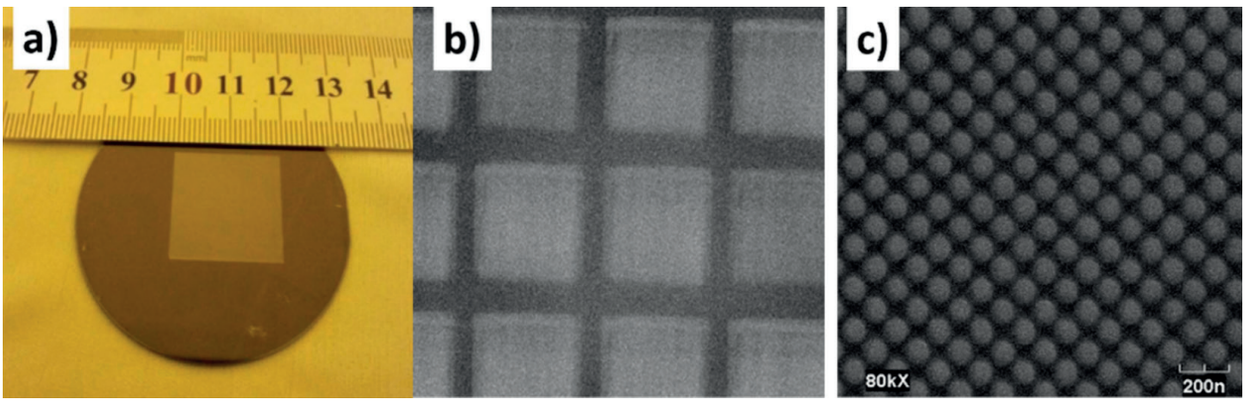

Figure 10. Large-area stitching exposure result: (a) 2 cm × 2 cm total exposure area; (b) stitched exposure blocks; (c) 120-nm period 2D nanostructures in a single block (reproduced from [18], with the permission of AIP publishing).

little impact for some applications for its smaller portion to the total exposure area. These 2D nanostructures show good uniformity with the period of 120 nm, as shown in **Figure 10c**.

4. Soft X-ray IL based on SR

At an EUV photon energy of 92.5 eV, it is difficult to obtain nanopatterns with high aspect ratio due to the strong absorption of conventional photoresist. Normally, the aspect ratio of usual nanopatterns done by EUV-IL is at most ~2 [21]. To improve the aspect ratio of the exposed nanopatterns, soft X-ray interference lithography (SXIL) with higher photon energy is recognized as a better method due to the higher transmission rate in photoresist. Soft X-ray interference lithography with higher photon energies, such as 190, 250 and 450, has already been employed for nanopattern fabrication with higher aspect ratios [12, 22]. High aspect ratio nanopatterns' exposure with high resolution and high uniformity are affected by the incident photon energy, the quality of the mask and the stability of the lithography system. Higher photon energy may decrease the whole optical efficiency of the system, resulting in

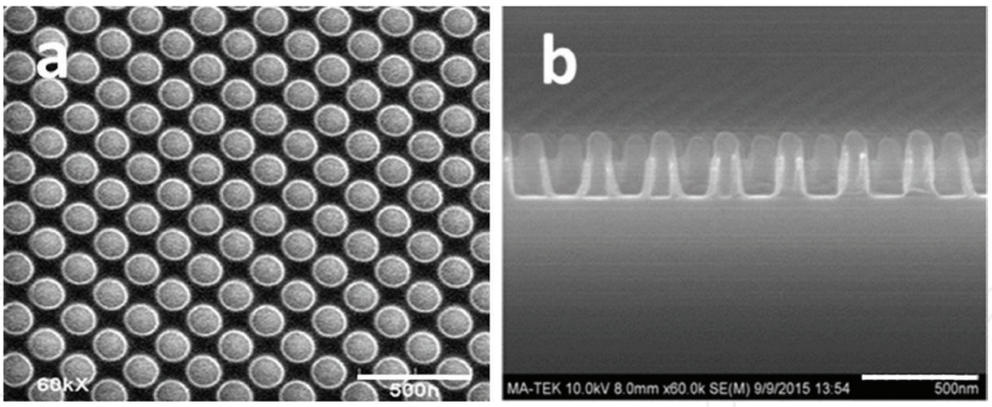

Figure 11. The SEM image of the SXIL exposure result (reproduced with permission from [23] ©2016 Elsevier B.V.).

lower photon flux. A high-absorbed layer is necessary during the exposure with higher photon energy, which makes the masks more fragile. To satisfy a high transmission rate in PMMA with balancing consideration of high photon flux, soft X-ray interference lithography (SXIL) at an energy of 140 eV was carried out at the XIL beamline (BL08U1B) at SSRF [23]. The nanohole array with 200-nm period was successfully obtained in a 300-nm thickness positive PMMA resist, **Figure 11a**. The aspect ratio of the pattern can be up to 3, **Figure 11b**. Compared with the EUV-IL, SXIL can provide a bigger process window for the latter pattern transfer process.

5. Applications

5.1. EUV photoresist evaluation

EUVL with a wavelength of 13.5 nm is thought to be the leading candidate for future nodes of high-volume semiconductor manufacturing. The most important challenges in EUVL include the EUVL system, mask and photoresist. ASML has made great progress toward the high-volume production of the EUVL system. The EUVL system, NXE:3350, is used to expose 1368 wafers per day. ASML expects the first IC manufacturers to start using EUV for chip production from 2018. EUV mask is an integral part of EUV lithography. Intel has installed its pilot production line for EUV mask manufacturing, fixing and detecting. In photolithography, a single defect ruins the chip. Defects on the EUV mask should be detected very clearly. Defects on the EUV mask can be detected by the scanning coherent diffractive imaging methods or by the high-resolution EUV Fresnel zone plate microscope [24].

Photoresist performance is one of the key parameters affecting the performance of EUVL. Due to the really high price of an EUVL system, it is not so easy to evaluate the new resist material by using the practical and affordable optical system. Available projection tools are usually used by researchers to invest in the performance of new resist. However, the resolution of these tools is limited due to the numerical aperture of the projection optics. Based on the coherent radiation from an undulator source, EUV-IL can be used to study the resolution (half pitch, HP), sensitivity (dose) and line-edge roughness of new EUV resist material. In addition to the main challenge of developing high-power EUV sources, EUV-IL has proved to be the best candidate for high-resolution EUV resist evaluation.

http://dx.doi.org/10.5772/intechopen.74564

EUV-IL enabled the characterization and development of new EUV resist materials before commercial EUV exposure tools became available. EUV resist has been performed on the EUV-IL beamline at SLS [25] and on the XIL beamline at SSRF [26]. Line structures of new EUV resist material with HP of 12 nm have been fabricated at the EUV-IL beamline at SLS, as shown in **Figure 12**. Line structures of new EUV resist material with LWR of 2 nm have been fabricated at the XIL beamline at SSRF, as shown in **Figure 13**. An outgassing test system has been built on the XIL beamline at SSRF too.

5.2. Nano-science

Surface-enhanced Raman scattering (SERS) [27, 28]: Surface-enhanced Raman scattering has been promisingly used in the field of biosensor fabrication with high sensitivity. The enhanced electromagnetic field which happens at the "hotspots" is intimately associated with the high sensitivity. Hotspots can be increased by increasing the density nanoarrays, tuning the shape of nanoparticles or reducing the nanogap between two nanoparticles. Due to its high density and uniformity, EUV-IL has been used for large-area SERS biosensor fabrication.

Large-scale Au nanodisk arrays have been produced on the XIL beamline at SSRF [27]. Nanohole arrays in a 200-nm period were fabricated on the PMMA resist, followed by the Au electron-beam vapor deposition. R6G as low as 10^{-8} M with an enhancement factor of 10^{6} has been detected on the Au nanodisk array. High sensitivity with high reproducibility and stability has been verified on the Au nanodisk arrays SERS-active substrates. A total of 32 spot SERS spectra were also collected on the Au nanodisk arrays. The values of RSD of vibrations 1313, 1366 and 1512 cm^{-1} are 18.1, 15.5 and 13.4%. Due to its high density and uniformity, XIL nanofabrication appears to be a promising method for SERS-active substrates' fabrication with high sensitivity and reproducibility.

Metal plasmonic nanostructures with sub-10-nm channels have been fabricated on the EUV-IL beamline at SLS [28]. The SERS signal can be increased by reducing the nanogap

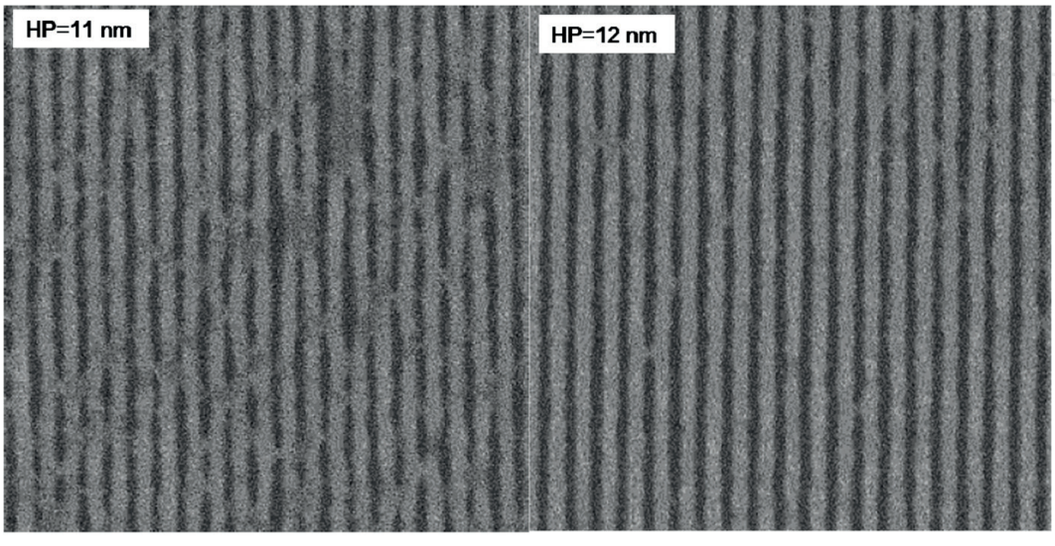

Figure 12. The EUV resist test result, done by XIL-II at SLS (reproduced with permission from [25] ©(2015) COPYRIGHT Society of Photo-Optical Instrumentation Engineers (SPIE)).

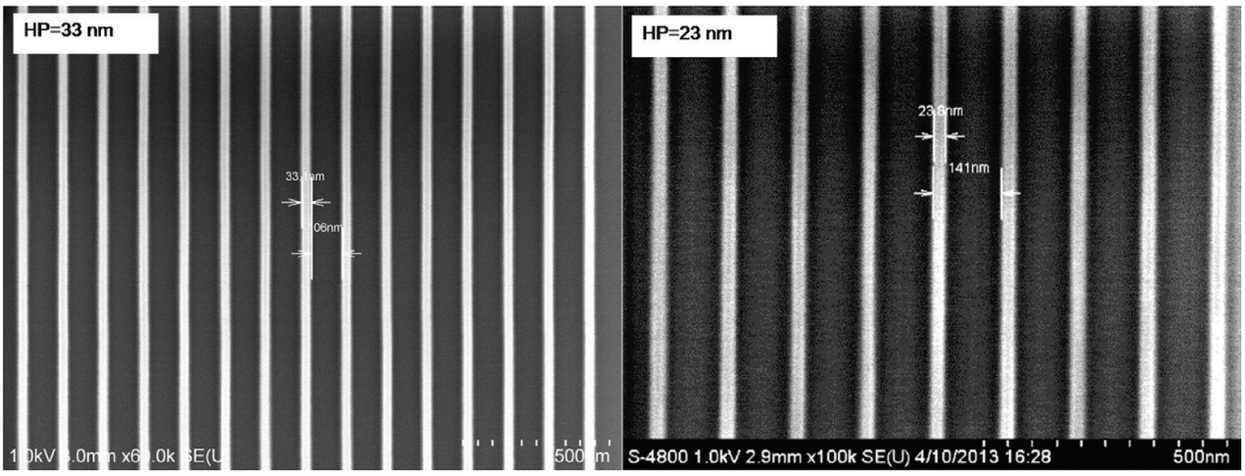

Figure 13. EUV resist test result done by XIL at SSRF.

between two nanoparticles. Double-layer plasmonic nanostructures were fabricated by depositing metal normally onto patterned photoresist layers, which were exposed at the EUV-IL beamline. Metal plasmonic nanostructures with sub-10-nm channels could be produced if the metal layer extended above the photoresist layer, as shown in **Figure 14**. By a comparison with the single-layer antenna, the Raman scattering signal of the double layers with sub-10-nm channels could be improved by a factor of 60. Period nanostructures with high resolution can be done by EUV-IL over a large area at a low cost. Followed by the extended metal layer deposition, high-sensitive SERS-active substrates can be obtained with low cost over large areas, which will be applicable in the near future.

Enhanced light extraction of scintillator [29]: Scintillators are usually used in the radiation detection system. Luminescence in ultraviolet or visible emission can be excited on scintillators by radiation from X-ray, c-ray, electrons, protons and neutrons. Periodic nanostructures over an area of 5.6 × 5.6 mm^2 have been fabricated on the surface of the Bi4Ge3O12 (BGO) scintillator

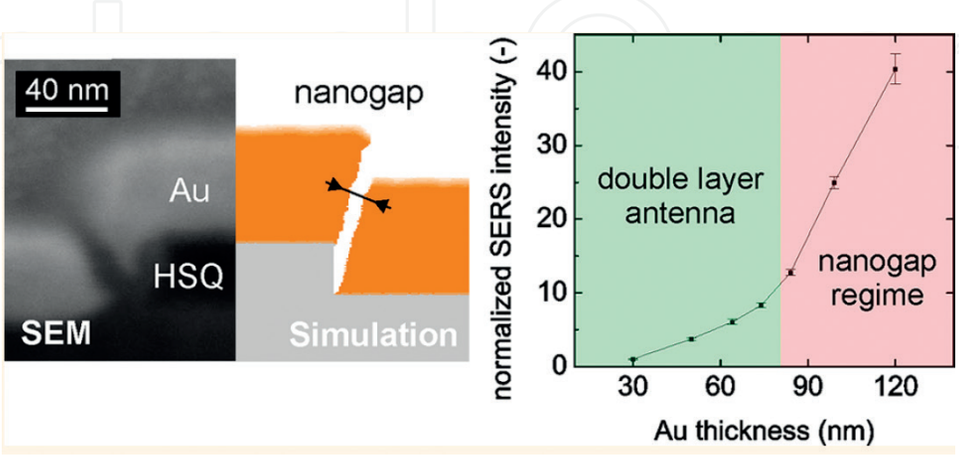

Figure 14. Ballistic simulation of the evaporated cross-section for a double-layer pattern with a nanogap channel (reproduced with permission from [28] ©2014 American Chemical Society).

by the four-beam stitching EUV-IL technique [18]. Combined with conformal deposition of TiO2 by atomic layer deposition, photonic crystal structures over a large area are fabricated. The emission spectra for this photonic crystal with different emergence angles under the excitation at 360 nm have been analyzed. An enhancement factor of 95.1% has been achieved. Photonic crystal structures with large-area and high-index contrast have been fabricated by this method.

Large-area plasmonic color filters [30]: Color filters based on plasmonic nanostructures have received prominent attention in recent years due to their capability of controlling the intensity, phase and polarization of light. Conventional lithography techniques such as electron beam lithography (EBL) and focused ion beam (FIB) are usually used for the plasmonic color filter fabrication. However, the small exposure area and the little throughput of these methods restrict their applications. By the four-beam stitching XIL technique, periodic hole arrays over large areas can be easily fabricated [18]. Followed by the e-beam evaporation of Ag, plasmonic color filters can be produced over large areas. The fill factor of nanostructures can be controlled by changing the dose of exposure. By changing the fill factor, the color can be controlled flexibly. **Figure 15** shows a blue filter device over a large scale fabricated by this method.

High-resolution Fresnel zone plate fabrication [31]: High-resolution Fresnel zone plates (FZPs) are often used in high-resolution x-ray microscopy. The resolution of the x-ray microscopy is limited to its outermost zone of the FZP which is used as a lens. EBL is usually used for the

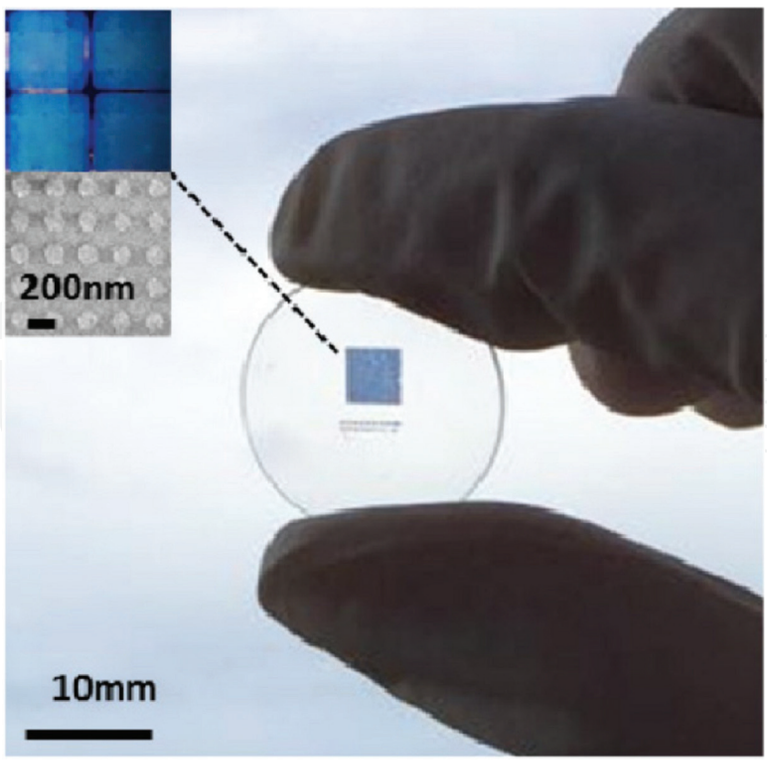

Figure 15. One blue filter device fabricated by stitching XIL, held by fingers (reproduced with permission from [30] ©2016 Optical Society of America).

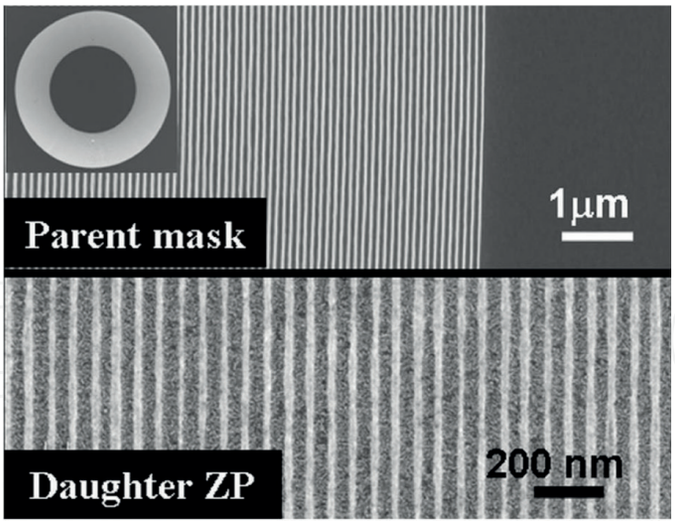

Figure 16. SEM images of the outer zones of a parent mask and the corresponding daughter ZP are shown in the SEM images. Inset shows the full ZP on the mask. (reproduced with permission from [31] ©2011 Optical Society of America).

FZP fabrication with high resolution. Based on the self-imaging (ASFM) property of gratings, high-resolution Fresnel zone plates (FZPs) have been fabricated on the EUV-Il beamline in PSI. ASFM is also known as ATL. Under wide-band illumination with spectral width $\Delta\lambda$, achromatic and stationary imaging of the original grating can be obtained beyond the distance $Z_A = 2P^2/\Delta\lambda$. Under broadband EUV illumination, a radially oscillating intensity distribution with double the spatial frequency of the parent ZP is produced. This intensity distribution is observed in a certain distance range, which can be used to record daughter ZPs with half the zone width of the parent ZPs. FZPs with zone widths as low as 30 nm have been fabricated, as shown in **Figure 16**. FZP fabrication with high resolution and high throughput can be fabricated in this way.

6. Conclusion(s)

Extreme UV interference lithography (EUV-IL) is a useful tool to fabricate periodic nanostructures and is considered as an ideal method for EUV photoresist evaluation. Synchrotron radiation beamlines provide stable sources with full spatial coherence, which are enough to support EUV-IL and necessary to further support soft X-ray interference lithography (SXIL) with higher photon energies. The diffraction schemes are limited to achromatic ones (SXIL) in usual multi-grating interference lithography because the synchrotron radiation beams have limited bandwidths. However, the limited bandwidth is essential to be employed in achromatic Talbot lithography (ATL) with a large focal length. Based on the two interference lithography methods, step-and-repeat ATL and stitching Multi-grating EUV-IL/SXIL have been developed to fabricate centimeter-scale periodic structures. Many nano-science applications have been illustrated, with EUV-IL as fabrication tools.

Acknowledgements

This work was supported by National Key R&D Program of China (2016YFA0401302),the National Natural Science Foundation of China (No. 11775291,11505275, 11475251,11275255), the Youth Innovation Promotion Association (No. 2017306), the Open Research Project of Large Scientific Facility from Chinese Academy of Sciences: Study on Self-Assembly Technology and Nanometer Array with Ultrahigh Density. The authors thank the support of BL08U1B and BL08U1A at SSRF for sample preparation. The authors also thank Dr. H.H. Solak (EULITHA AG) and Dr. Y. Ekinci (XIL-II, SLS) for helpful discussions on EUV-IL and ATL. Parts of this chapter are taken from the authors' former work at the SSRF beamline BL08U1B [2], on ATL [15, 16], SXIL [23] and stitching multi-grating EUV-IL/SXIL [17, 18] and parts of the nano-science applications of EUV-IL are taken from [27–31].

Conflict of interest

I confirm there are no conflicts of interest.

Author details

Shumin Yang and Yanqing Wu*

*Address all correspondence to: wuyanqing@sinap.ac.cn

Shanghai Institute of Applied Physics, Shanghai Synchrotron Radiation Facility, Shanghai, China

References

[1] Buitrago E, Fallica R, Fan D, Karim W, Vockenhuber M, van Bokhoven AJ, Ekinci Y. From powerful research platform for industrial EUV photoresist development, to world record resolution by photolithography: EUV interference lithography at the Paul Scherrer Institute. Proceedings of SPIE. 2016;**9426**:94260T-12. DOI: 10.1117/12.2238805

[2] Yang SM, Wang LS, Zhao J, Xue CF, Liu HG, Xu ZJ, Wu YQ, Tai RZ. Developments at SSRF in soft X-ray interference lithography. Nuclear Science and Techniques. 2015;**26**:010101-010107. DOI: 10.13538/j.1001-8042/nst.26.010101

[3] Fukushima Y, Sakagami N, Kimura T, Kamaji Y, Iguchi T, Yamaguchi Y, Tada M, Harada T, Watanabe T and Kinoshita H. Development of extreme ultraviolet interference lithography system. Japanese Journal of Applied Physics. 2010;**49**:06GD06-06GD05. DOI: 10.1143/JJAP.49.06GD06

[4] Isoyan A, Wüest A, Wallace J, Jiang F, Cerrina F. 4X reduction extreme ultraviolet interferometric lithography. Optics Express. 2008;**16**:9106-9111. DOI: 10.1364/OE.16.009106

[5] Lin CH, Fong CH, Lin YM, Lee YY, Fung HS, Shew BY, Shieh J. EUV interferometric lithography and structural characterization of an EUV diffraction grating with nondestructive spectroscopic ellipsometry. Microelectronic Engineering. 2011;**88**:2639-2643. DOI: 10.1016/j.mee.2011.02.002

[6] Solak HH, He D, Li W, Singh-Gasson S, Cerrina F, Sohn BH, Yang XM, Nealey P. Exposure of 38 nm period grating patterns with extreme ultraviolet interferometric lithography. Applied Physics Letters. 1999;**75**:2328-2330. DOI: 10.1063/1.125005

[7] Solak HH, Li W, He D, Wallace J, Cerrina F. A new beamline for EUV lithography research. AIP Conference Proceedings. 2000;**521**:99-103. DOI: 10.1063/1.1291766

[8] Auzelyte V, Dais C, Farquet P, Grützmacher D, Heyderman LJ, Luo F, Olliges S, Padeste C, Sahoo PK, Thomson T, Turchanin A, David C, Solak HH. Extreme ultraviolet interference lithography at the Paul Scherrer Institut. Journal of Micro/Nanolithography, MEMS, and MOEMS. 2009;**8**(2):021204-0212010. DOI: 10.1117/1.3116559

[9] Solak HH, David C, Gobrecht J, Wang L, Cerrina F. Multiple-beam interference lithography with electron beam written gratings. Journal of Vacuum Science & Technology B: Microelectronics and Nanometer Structures Processing, Measurement, and Phenomena. 2002;**20**(6):2844-2848. DOI: 10.1116/1.1518015

[10] Solak HH. Space-invariant multiple-beam achromatic EUV interference lithography. Microelectronic Engineering. 2005;**78-79**:410-416. DOI: 10.1016/j.mee.2005.01.012

[11] Solak HH. Nanolithography with coherent extreme ultraviolet light. Journal of Physics D: Applied Physics. 2006;**39**:R171-R188. DOI: 10.1088/0022-3727/39/10/R01

[12] Mojarad N, Gobrecht J, Ekinci Y. Interference lithography at EUV and soft X-ray wavelengths: Principles, methods, and applications. Microelectronic Engineering. 2015;**143**: 55-63. DOI: 10.1016/j.mee.2015.03.047

[13] Talbot HF. Facts relating to optical science No. IV. The London, Edinburgh, and Dublin Philosophical Magazine and Journal of Science. 1836;**9**(56):403-407. DOI: 10.1080/14786443608649032

[14] Guérineau N, Harchaoui B, Primot J. Talbot experiment re-examined: Demonstration of an achromatic and continuous self-imaging regime. Optics Communications. 2000;**180**:199-203. DOI: 10.1016/S0030-4018(00)00717-3

[15] Yang SM, Zhao J, Wang LS, Zhu FY, Xue CF, Liu HG, Wu YQ, Tai RZ. Influence of symmetry and duty cycles on the pattern generation in achromatic Talbot lithography. Journal of Vacuum Science & Technology B. 2017;**35**(2):021601-021607. DOI: 10.1116/1.4974930

[16] Fan D, Buitrago E, Yang SM, Karim W, Wu YQ, Tai RZ, Ekinci Y. Patterning of nanodot-arrays using EUV achromatic Talbot lithography at the Swiss Light Source and Shanghai Synchrotron Radiation Facility. Microelectronic Engineering. 2016;**155**:55-60. DOI: 10.1016/j.mee.2016.02.026

[17] Karim W, Tschupp SA, Oezaslan M, Schmidt JT, Gobrecht J, Bokhoven JA, Ekinci Y. High-resolution and large-area nanoparticle arrays using EUV interference lithography. Nanoscale 2015;**7**:7386-7393. DOI: 10.1039/c5nr00565e

[18] Xue CF, Wu YQ, Zhu FY, Yang SM, Liu HG, Zhao J, Wang LS, Tai RZ. Development of broadband X-ray interference lithography large area exposure system. Review of Scientific Instruments. 2016;**87**:043303-043304. DOI: 10.1063/1.4947067

[19] Xue C, Zhao J, Wu YQ, Yu HN, Yang SM, Wang LS, Zhao WC, Wu Q, Zhu ZC, Liu B, Zhang X, Zhou WC, Tai RZ. Fabrication of large-area high-aspect-ratio periodic nanostructures on various substrates by soft X-ray interference lithography. Applied Surface Science. 2017;**425**:553-557. DOI: 10.1016/j.apsusc.2017.07.010

[20] Wang L, Solak HH, Ekinci Y. Fabrication of high-resolution large-area patterns using EUV interference lithography in a scan exposure mode. Nanotechnology 2012;**23**:305303-305305. DOI: 10.1088/0957-4484/23/30/305303

[21] Solak HH, David C, Gobrecht J, Wang L, Cerrina F, Four-wave E. UV interference lithography. Microelectronic Engineering. 2002;**61-62**:77-82. DOI: 10.1016/S0167-9317(02)00579-8

[22] Mojarad N, Fan D, Gobrecht J, Ekinci Y. Broadband interference lithography at extreme ultraviolet and soft X-ray wavelengths. Optics Letters. 2014;**39**(8):2286-2289. DOI: 10.1364/OL.39.002286

[23] Zhao J, Wu YQ, Xue CF, Yang SM, Wang LS, Zhu FY, Zhu ZC, Liu B, Wang Y, Tai RZ. Fabrication of high aspect ratio nanoscale periodic structures by the soft X-ray interference lithography. Microelectronic Engineering. 2017;**170**:49-53. DOI: 10.1016/j.mee.2016.12.028

[24] Helfenstein P, Mohacsi I, Rajeev R, Ekinci Y. Scanning coherent diffractive imaging methods for actinic extreme ultraviolet mask metrology. Journal of Micro/Nanolithography, MEMS, and MOEMS. 2016;**15**(3):034006-034005. DOI: 10.1117/JMM.15.3.034006

[25] Buitrago E, Yildirim O, Verspaget C, Tsugama N, Hoefnagels R, Rispens G, Ekinci Y. Evaluation of EUV resist performance using interference lithography. Proceedings of SPIE. 2015;**9422**:94221S-1-94221S-13. DOI: 10.1117/12.2085803

[26] Chen L, Xu J, Yuan H, Yang SM, Wang LS, Wu YQ, Zhao J, Chen M, Liu HG, Li SY, Tai RZ, Wang SQ, Yang GQ. Outgassing analysis of molecular glass photoresists under EUV irradiation. Science China Chemistry. 2014;**57**(12):1746-1750. DOI: 10.1007/s11426-014-5122-y

[27] Zhang PP, Yang SM, Wang LS, Zhao J, Zhu ZC, Liu B, Zhong J, Sun XH. Large-scale uniform Au nanodisk arrays fabricated via X-ray interference lithography for reproducible and sensitive SERS substrate. Nanotechnology. 2014;**25**:245301-245308. DOI: 10.1088/0957-4484/25/24/245301

[28] Siegfried T, Wang L, Ekinci Y, Martin QJF, Sigg H. Metal double layers with Sub-10 nm channels. ACS Nano. 2014;**8**(4):3700-3706. DOI: 10.1021/nn500375z

[29] Zhu ZC, Wu S, Xue CF, Zhao J, Wang LS, Wu YQ, Liu B, Cheng CW, Gu M, Chen H, Tai RZ. Enhanced light extraction of scintillator using large-area photonic crystal structures fabricated by soft-X-ray interference lithography. Applied Physics Letters. 2015;**106**:241901-241905. DOI: 10.1063/1.4922699

[30] Sun LB, Hu XL, Wu QJ, Wang LS, Zhao J, Yang SM, Tai RZ, Fecht HJ, Zhang DX, Wang LQ, Jiang JZ. High throughput fabrication of large-area plasmonic color filters by soft-X-ray interference lithography. Optics Express. 2016;**24**(17):19112-19121. DOI: 10.1364/OE.24.019112

[31] Sarkar SS, Solak HH, Saidani M, David C, Friso van der Veen J. High-resolution Fresnel zone plate fabrication by achromatic spatial frequency multiplication with extreme ultraviolet radiation. Optics Letters. 2011;**36**(10):1860-1862. DOI: 10.1364/OL.36.001860